Phase relaxation control in heterostructures featuring charge-transfer excitons

M. Fey,[1] M. Stein,[1,*] C. Fuchs,[2] W. Stolz,[2] K. Volz,[2] and S. Chatterjee[1]

[1]*Institute of Experimental Physics I and Center for Materials Research (LaMa), Justus-Liebig-Universität Gießen, Heinrich-Buff-Ring 16, 35392 Gießen, Germany*

[2]*Department of Physics and Material Sciences Center, Philipps-Universität Marburg, Renthof 5, 35032 Marburg, Germany*

(Received 17 May 2022; revised 27 August 2022; accepted 27 September 2022; published 10 October 2022)

Type-II quantum well heterostructures are considered high-potential candidates for next-generation active semiconductor devices. They promise low fundamental transition energies and suppressed Auger scattering as well as temperature stability in device performance. Understanding their fundamental properties, such as scattering and diffusion, and revealing intricate differences from type-I quantum structures are important steps towards optimized structure design. Using degenerate four-wave mixing spectroscopy, we investigate the phase coherence of excitonic polarizations in a (Ga,In)As/GaAs/Ga(As,Sb) type-II double-quantum-well structure. It is designed to exhibit spectrally isolated resonances in its linear absorption spectrum including a well-resolved charge-transfer exciton resonance. This allows us to study the coherent dynamics of the unperturbed charge-transfer exciton polarization. In addition, the effects of many-body interactions with free charge carriers as well as excitons that are injected by an optical prepulse are revealed. Scattering of charge-transfer excitons with free charge carriers is three times more efficient than scattering of charge-transfer excitons with each other. The comparison with Wannier excitons in a type-I quantum well structure shows that the interaction strength between charge-transfer excitons is about twice as large as for excitons in a type-I quantum well structure.

DOI: 10.1103/PhysRevB.106.165303

I. INTRODUCTION

Most modern electrical and optoelectronic devices consist of complex semiconductor heterostructures. These are continuously decreased in size yet increase in complexity due to the advancing miniaturization of solid-state devices. They often comprise hundreds of individual layers with thicknesses in the nanometer regime [1,2]. Consequently, the properties of internal interfaces between different semiconductor materials are increasingly important, as they affect their electro-optical properties and, consequently, the device performances [3,4].

So-called type-II quantum well (QW) heterostructures are a promising system to study the influence of internal interfaces on the charge-carrier dynamics [5–7]. In such systems, the conduction band minimum and the valence band maximum are localized on different sides of an internal interface. The attractive interaction between electrons and holes may cause the formation of excitons that are indirect in real space, commonly termed charge-transfer excitons (CTXs). These CTXs are perfect sensors for the investigation of interface properties as they are delocalized across internal interfaces. Unfortunately, the weak overlap of the composite electron and hole wave functions and resulting low oscillator strengths render them rarely accessible to absorption spectroscopy, hindering direct optical excitation of coherent CTXs [8]. Consequently, virtually exclusively the spatially direct transitions in type-II-like structures have been studied via four-wave mixing (FWM) spectroscopy in the past [9–11]. The spatially indirect transitions have only been accessible via photoluminescence spectroscopy, which is more readily amenable to the lowest-energy transitions [12,13]. However, the sophisticated sample design consisting of a (Ga,In)As and a Ga(As,Sb) layer separated by an extremely thin GaAs interlayer and encapsulated by GaAs barriers allows for the observation of a CTX resonance in the linear absorption spectrum [14,15]. This enables resonant excitation of CTXs and, thus, detailed analysis of their previously inaccessible coherent dynamics.

In this paper, we investigate the coherent dynamics of CTXs in a type-II quantum well structure by four-wave mixing spectroscopy. In particular, we report on the phase coherence of a CTX polarization in the presence of incoherent populations of excitons or free carriers that are injected by an additional prepulse. Analyzing the phase coherence time T_2 in terms of the present charge-carrier density reveals the collision-rate parameters for collisions between a CTX polarization and either incoherent CTXs or spatially separated incoherent charge carriers. The comparison with experiments on a type-I quantum well structure reveals the specific characteristics related to the spatially indirect nature of electrons and holes in the type-II quantum well sample: Exciton-exciton scattering is more efficient for CTXs than for their counterparts in type-I quantum wells. This is tentatively ascribed to the larger fermionic character of the CTXs compared with the Wannier-type excitations in type-I quantum wells due to the delocalization across the interface.

II. SAMPLE DESIGN

The four-wave mixing experiments are performed on two different quantum well heterostructures grown by metal organic vapor phase epitaxy in an AIXTRON AIX 200 Gas Foil

*markus.stein@exp1.physik.uni-giessen.de

TABLE I. The homogeneous (Γ_{homo}) and inhomogeneous (Γ_{inhomo}) linewidth of the different excitonic absorption peaks in the type-I and type-II samples derived from Voigt fits. The phase coherence time T_2 corresponding to the homogeneous linewidth is calculated via $T_2 = \frac{2\hbar}{\Gamma_{\text{homo}}}$.

	Γ_{homo} (meV)	Γ_{inhomo} (meV)	T_2 (ps)
Type-I (Ga,In)As	0.76	1.54	1.73
Type-II (Ga,In)As	2.2	2.0	0.6
Type-II Ga(As,Sb)	3.9	3.2	0.34
Type-II CTX	2.1	4.0	0.63

Rotation (GFR) reactor system. We use tertiary butylarsine (TBA), tertiary butylphosphine (TBP), and triethylantimony (TESb) as group V precursors, while triethylgallium (TEGa) and trimethylindium (TMIn) are used as group III precursors. The samples have been grown at a growth temperature of 500 °C on a GaAs (001) substrate.

The active layer of the type-II system consists of 50 repetitions of compressively strained (Ga,In)As/GaAs/Ga(As,Sb) layers separated by tensilely strained GaAs/GaAsP/GaAs barriers which provide strain compensation on the GaAs substrates. High-resolution x-ray diffraction and atomic force microscopy yield well thicknesses of 7.7 nm [(Ga,In)As] and 7.5 nm [Ga(As,Sb)], an interlayer thickness of 1 nm, and In and Sb concentrations of 5.8 and 7%, respectively [15]. Here, the low In and Sb concentrations provide shallow (only a few tens of meV deep) quantum wells. The combination of shallow quantum wells with a very thin interlayer guarantees a comparatively large reach-in of the electron and hole wave functions into the neighboring quantum well layer, resulting in a large wave function overlap between the (Ga,In)As quantum well electron and Ga(As,Sb) quantum well hole wave functions.

The individual (Ga,In)As and Ga(As,Sb) quantum wells give rise to different resonances in the linear absorption spectrum at 1.46 and 1.44 eV which are assigned to the respective exciton resonances [see Fig. 1(b)]. Due to the high sample quality and the comparatively small linewidth for ternary quantum structures, an additional resonance in the linear absorption can be identified at 1.4 eV. This resonance at 1.4 eV, having the lowest transition energy, is associated with the spatially indirect CTX transition.

A multiple-quantum-well structure containing 50 (Ga,In)As layers separated by barriers similar to the above barriers is grown under comparable conditions. This type-I reference structure features only a single resonance at 1.46 eV which is also observed in the type-II sample. It is therefore unambiguously assigned to the (Ga,In)As quantum well. Voigt fits to the individual exciton resonances in the linear absorption spectrum indicate that the lowest-energy transitions in both samples are mainly inhomogeneously broadened (see Table I).

III. EXPERIMENTAL DETAILS

A 1-MHz repetition rate regenerative amplifier system provides 190-fs pulses centered at 1.2 eV which drive an optical

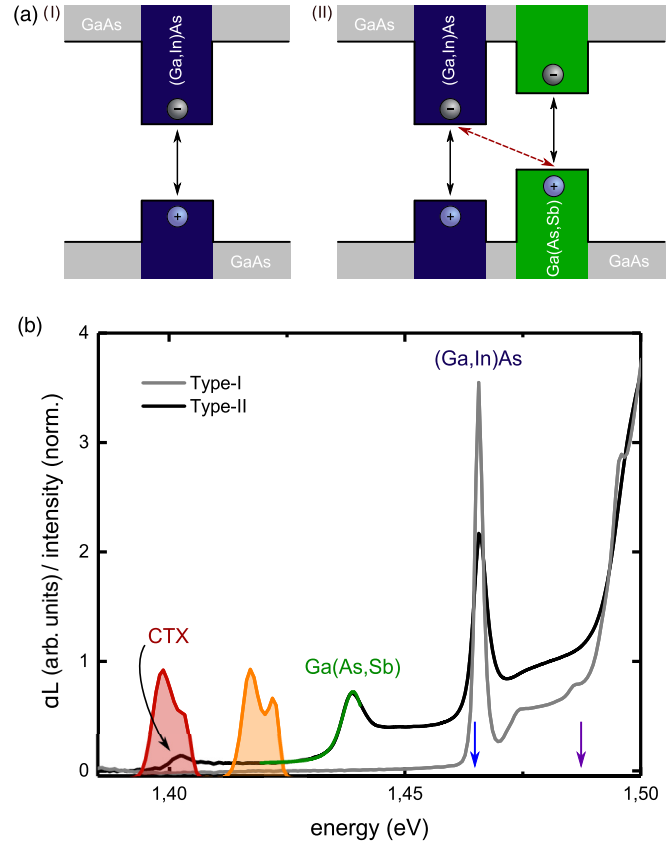

FIG. 1. (a) Schematic band scheme of the reference sample (left) and the type-II system (right). The reference sample has a spatially direct transition (black arrows) within the (Ga,In)As layers. The lowest-energy transition in the type-II heterostructure is spatially indirect (red arrow). (b) Linear absorption of the reference sample (gray) and type-II heterostructure (black) at a temperature of 6 K. The spectra in red and orange indicate the photon energies of prepulses injecting excitons or free charge carriers in the type-II structure, while the arrows in blue and purple indicate the corresponding prepulse photon energies used in the reference sample. A Voigt fit (green curve) is exemplarily applied to the excitonic resonance at 1.44 eV.

parametric amplifier emitting tuneable, broadband pulses with a duration of 50 fs. The FWM experiments are performed in a two-beam self-diffraction geometry, where pulse 1 with wave vector $\vec{k}_1$ injects a polarization into the samples, which are held at 6 K in vacuum on a cold finger helium flow cryostat. Subsequently, pulse 2 with wave vector $\vec{k}_2 \neq \vec{k}_1$ impinges on the sample with a time delay T_{12} and interacts with the remaining polarization present in the sample (Fig. 2). The interaction leads to the formation of an interference grating as long as the time delay between the two pulses is smaller than the phase coherence time T_2 of the initially injected polarization. As a result, a part of the second pulse self-diffracts off the grating into the $\vec{k}_2$-$\vec{k}_1$ direction. The dependence of the diffracted signal on the time delay T_{12} directly monitors the phase relaxation [16].

Furthermore, we use FWM experiments to study scattering processes between a coherent exciton polarization and incoherent excitons as well as free carriers since their interactions affect the phase coherence [9,17,18]. For this

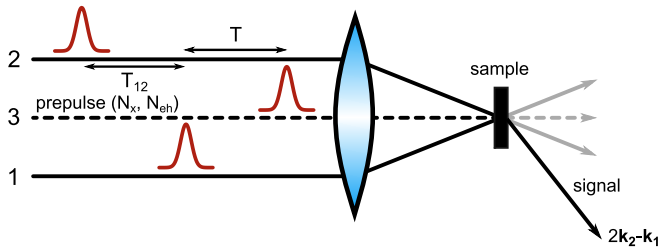

FIG. 2. Schematic illustration of the four-wave mixing setup in a self-diffraction geometry. The prepulse (advanced by T) injects either free carriers or excitons. Pulses 1 and 2 delayed by T_{12} form a transient interference grating. The self-diffracted FWM signal monitors the phase relaxation of the exciton polarization.

purpose, a prepulse (pulse 3) from the optical parametric amplifier is spectrally tailored using band-edge filters. It injects either free carriers or excitons before pulse 1 impinges on the sample ($T < 0$). Excitons are generated by resonant excitation of the energetically lowest exciton resonance. As shown by Stein *et al.* [14], these excitation conditions build an exciton population within a few picoseconds in type-I as well as type-II samples. Accordingly, time leads of $T = -10$ ps and $T = -4$ ps of the prepulse are ideally suited to resonantly prepare an incoherent heavy-hole (hh) exciton population in the type-I sample and the type-II sample, respectively. The larger temporal lead of the prepulse in the type-I sample is chosen because of the longer coherence time in this sample compared with the type-II sample.

Free electrons and holes are generated by a prepulse which is energetically above the excitonic resonance. In this scenario, it takes dozens of picoseconds for a significant exciton population to build up [14]. At the same time, coherence is lost almost instantaneously under these nonresonant excitation conditions. Consequently, a time lead of $T = -1$ ps is perfect for preparing a population of free electrons and holes in both samples. With the individually selected lead times, we ensure that all excitations from the various prepulses have lost any coherence once the four-wave mixing pulses arrive and, consequently, provide incoherent scattering partners. A photodiode measures the time-integrated FWM signal as a function of the delay time between pulses 1 and 2. We choose the excitation intensity of pulse 1 so that it will be as low as possible to obtain a long phase coherence close to the respective zero-density phase coherence time of the resonance. The phase coherence time T_2 is obtained by an exponential fit to the time decay of the measured diffracted signal. All pulses are circularly polarized by $\lambda/4$ plates. This, in particular, avoids quantum beats in the time-integrated FWM signal.

The photoinduced carrier density has been estimated from the pulse spectrum and the linear absorption of the sample as well as by power measurements of the pulse before and after passing through the sample, assuming realistic reflection losses. The spot size on the sample was determined using a camera-based beam profiler. Both methods provided a consistent picture of the charge-carrier density.

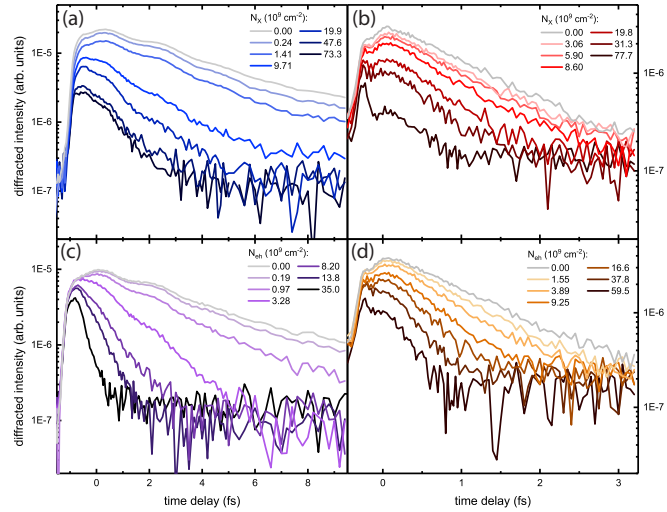

FIG. 3. FWM transients of the reference sample (left column) and the type-II system (right column) in the presence of additional incoherent excitons [(a) and (b)] and free charge carriers [(c) and (d)].

IV. RESULTS

A. FWM signals of type-I and type-II structures

Figure 3 shows the intensity of the FWM signals from type-I (left column) and type-II (right column) structures as a function of the delay time T_{12}. For reference, the gray curves show the decay of the measured signal without a prepulse. The exponential fit to the measured diffracted curve of the type-II sample yields a decay time of $T_{\mathrm{Decay}} = 1.03$ ps when no prepulse is present. Since the exciton resonance is predominantly inhomogeneously broadened as shown in Table I, we calculate the phase coherence time T_2 from the decay time according to $T_2 = 4T_{\mathrm{Decay}}$ [19]. Thus we find a phase coherence time of a CTX polarization of $T_2 = 4.12$ ps in the low-density regime; we derive a phase coherence time of $T_2 = 15.12$ ps for the type-I reference structure and similar conditions. Accordingly, the coherent ensemble of CTXs decays more than three times faster than the exciton polarization in the type-I quantum well reference sample, which is similar to the result given by Stein *et al.* [14]. Accordingly, we attribute the faster decay of the CTX polarization to additional scattering processes at fluctuations in the material compositions of the quantum wells as well as scattering at internal interfaces. Since the CTX is distributed over three different material compositions, crosses four interfaces, and has a larger Bohr radius than a regular exciton, it is more susceptible to scattering processes.

Please note that the homogeneous linewidth of the two resonances also differs by about a factor of 3 as shown in Table I. However, the T_2 times resulting from the homogeneous linewidths of 1.73 and 0.63 ps for the type-I and the type-II samples, respectively, are almost an order of magnitude smaller than the phase coherence times determined via FWM. This suggests that broadening mechanisms other than the phase coherence time also affect the homogeneous linewidth of the samples [18]. Consequently, the homogeneous linewidth from the linear absorption is not a suitable quantity to derive the phase coherence time. Prepulses

detuned into the continuum generate free charge carriers, i.e., an electron-hole plasma (EHP). The respective photon energies are chosen such that the energies in excess of the lowest-energy transitions are comparable between the two samples. In particular, we excite the type-I structure 22 meV above the direct exciton resonance and the type-II heterostructure 19 meV above the spatially indirect CTX resonance as indicated by the purple arrow and orange pulse spectrum in Fig. 1(b), respectively. The prepulses are spectrally tailored by band-edge filters to prevent any resonant excitation of excitons within the quantum wells. As the carrier density N_{eh} increases, both the amplitude and the decay time of the diffracted signals in Figs. 3(c) and 3(d) decrease significantly. While the amplitude of the diffracted signal is reduced by the prepulse-induced bleaching of the excitonic resonances in the absorption, the decay time decreases due to excitation-induced dephasing (EID) [20,21]. The coherence time T_2 in the low-density regime ($N_{eh} = 0$) is mainly determined by the interaction with (acoustic) phonons and disorder potentials. Collisions between an exciton polarization and free carriers occur in the presence of additional carriers created by the prepulse [18]. Such scattering processes destroy the exciton phase coherence and, consequently, cause a reduction of the phase coherence time T_2.

For resonant excitation, we also use spectrally narrow pulses indicated in blue and red for the type-I structure and the type-II structure, respectively. Both pulses are spectrally narrowed by band-edge filters to avoid an excitation of an EHP. The decay of the FWM signals for both samples is shown in Figs. 3(a) and 3(b). Decay times decrease with the excitation density injected by the prepulses. Clearly, scattering with both free carriers and incoherent excitons leads to a faster loss of phase coherence at the exciton resonance in both samples.

We quantify these results by applying an exponential fit to all curves and calculating the associated homogeneous linewidth. The data are summarized as a function of the excitation density of the prepulse in Fig. 4.

B. Collision-rate parameter

Figure 4 compares the homogeneous linewidths Γ of the type-I (blue and purple spheres) and type-II (red and orange spheres) structures for different free carrier and exciton densities injected by the prepulse. In all cases, Γ increases linearly with density. For low excitation densities, the homogeneous linewidth is given by [18]

$$\Gamma(N_{eh,X}) = \Gamma_0 + \gamma a_{\mathrm{exc}}^2 E_B N_{eh,X}. \quad (1)$$

Here, a_{exc} is the exciton Bohr radius, and E_B is the exciton binding energy. The dimensionless parameter Γ_0 accounts for all scattering processes involving phonons, impurities, interfacial roughness, or compositional fluctuations within the quantum wells. The collision-rate parameter γ is a measure of the interaction strength between an exciton polarization and additional carriers injected by the prepulse. The slopes in Fig. 4 directly reflect the collision-rate parameter for scattering with incoherent excitons ($\gamma_{X\text{-}X}$) or free electrons and holes ($\gamma_{X\text{-}eh}$). To calculate γ, we use 7.9 and 3.6 meV as the exciton binding energies, i.e., 9/8 times the $1s$-$2p$ transition energy of structurally similar heterostructures [14], and 9.95 and 14.8 nm as the two-dimensional Bohr radius for the type-I and type-II samples, respectively [14].

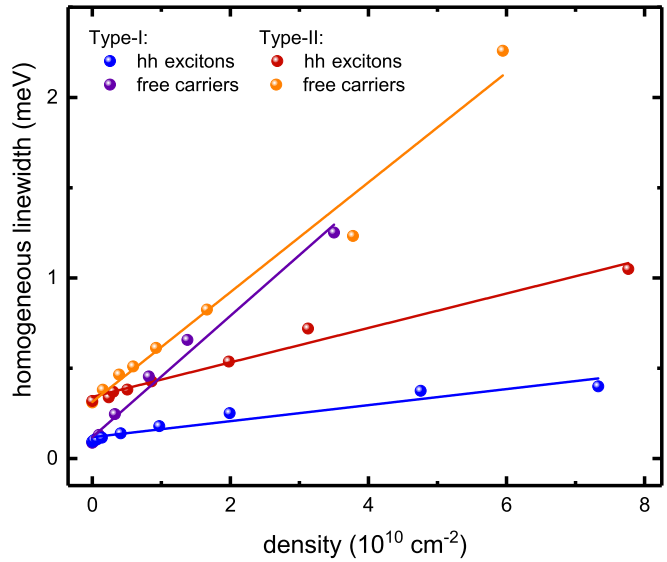

FIG. 4. Homogeneous linewidths of regular exciton (blue, purple) and CTX (red, orange) resonances as a function of the exciton and free-charge-carrier densities generated by the different prepulses. A linear regression of the measured data (solid lines) is used to derive the respective collision-rate parameters.

We find the interaction strength γ between an exciton polarization and incoherent excitons to be more efficient by a factor of 2 in the type-II heterostructure. We explain the larger interaction strength among CTXs by the spatial separation of electrons and holes within the active region of the type-II sample. Due to the carrier separation, CTXs have smaller binding energies and larger Bohr radii than Wannier excitons in spatially direct quantum well structures. Correspondingly, the spatial separation results in larger spatial dipole moments leading to an enhanced dipole-dipole interaction. Moreover, the larger Bohr radius may induce the spatially indirect CTX to be more sensitive to its fermionic substructure and thus to Pauli repulsion [14]. Both a larger spatial dipole moment and the Pauli repulsion increase the interaction strength between CTX compared with regular excitons and correspondingly enhance X-X scattering in the type-II double quantum wells.

For the reference sample, we find a collision-rate parameter of $\gamma_{X\text{-}X} = 0.56$ for incoherent excitons and $\gamma_{X\text{-}eh} = 4.3$ for free carriers. Thus free carriers attenuate the exciton phase coherence by a factor of about 8 (7.7) more efficiently than incoherent excitons. These data are extremely comparable to findings on a 12-nm GaAs single quantum well which show an eight-times-stronger interaction between an exciton polarization and free carriers [18]. Collisions with free carriers are more effective because of the long-range nature of the Coulomb interaction. In contrast to free electrons and holes, excitons are electrically virtually neutral quasiparticles. They interact with each other via the weaker dipole interaction [9,17,18]. For the type-II structure, we find a collision-rate parameter of $\gamma_{X\text{-}X} = 1.2$ for incoherent excitons and $\gamma_{X\text{-}eh} = 3.86$ for free carriers. Collisions with an EHP in type-II structures contribute to the loss of the CTX phase coherence more

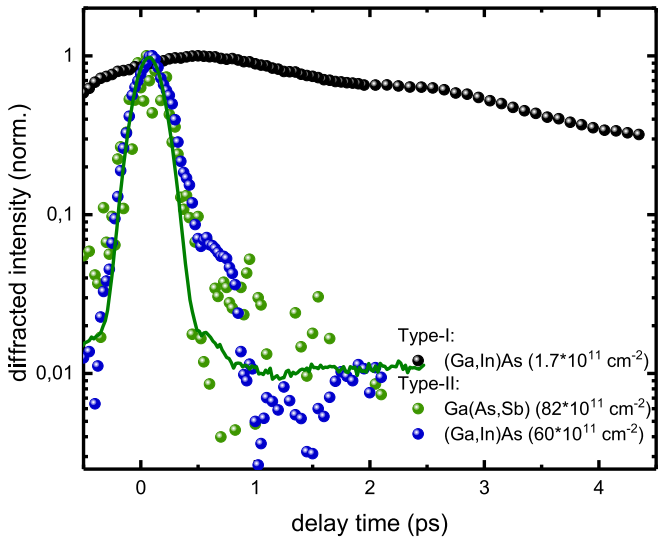

FIG. 5. FWM transients for resonant excitation of the exciton resonances of the (Ga,In)As (blue spheres) and Ga(As,Sb) (green spheres) quantum wells in the type-II heterostructure with photon densities of 6×10^{12} and 8.2×10^{12} cm^{-2}, respectively. The FWM transient of the resonantly excited type-I sample (black spheres) with a photon density of 1.7×10^{11} cm^{-2} is given for reference. The solid green curve represents the autocorrelation of the excitation pulses centered around the Ga(As,Sb) resonance.

effectively than collisions with incoherent CTX, similar to the results of type-I structures.

Notably, the collision-rate parameters $\gamma_{X\text{-}eh}$ of the reference sample and the type-II sample are very similar. The respective interaction strengths appear to be driven mainly by the EHP rather than by the particular nature of the exciton polarization. Furthermore, even the spatial separation of the electrons and holes of the EHP in the type-II sample does not significantly affect the scattering efficiency.

C. Spatially direct exciton polarizations in the type-II quantum well

Next, we turn to the coherent dynamics of regular excitons resonantly excited in the type-II sample. We use spectrally narrow pulses centered around the excitonic resonance of either the (Ga,In)As [blue arrow in Fig. 1(b)] or Ga(As,Sb) quantum well. Figure 5 shows the FWM transients for both spatially direct excitations of Wannier excitons in the type-II structure. Both FWM signals exhibit a very fast decay that is almost independent of the excitation density. Furthermore, the diffracted signals are extremely small and hardly detectable. Accordingly, comparatively high photon densities are required, despite the pronounced exciton resonances in the linear absorption spectra. The symmetry of the diffracted signals and the low signal intensity suggest that the phase coherence time of the associated exciton polarizations is much shorter than the pulse duration. Consequently, the coherent polarization decays to a large extent while the optical pulse is still present, so that hardly any coherence builds up. Accordingly, the curve of the diffracted signals strongly resembles the autocorrelation measurements of the corresponding pulses, as exemplified by the green curve in Fig. 5. A comparison with the FWM signal from resonant excitation of the reference sample (black spheres in Fig. 5) shows that regular exciton polarizations decay orders of magnitude faster in the presence of a lower-energy state which is given by the type-II structure. Therefore we attribute the ultrafast loss of regular exciton coherence in the type-II system to relaxation processes into states at lower energies by Coulomb scattering. Those relaxation processes are accompanied by a charge transfer of either electrons or holes into the adjacent layers, resulting in a fast destruction of the phase coherence in a time range of a few hundred femtoseconds. This observation is consistent with the terahertz emission observed by the fast charge transfer in structurally similar samples [15,22]. Furthermore, it is consistent with the observed homogeneous linewidths of the excitonic transitions. The homogeneous linewidths from Table I correspond to phase coherence times of 0.6 and 0.34 ps of the (Ga,In)As exciton resonance and the Ga(As,Sb) exciton resonance, respectively, which should lead to FWM dephasing times in a range between 85 and 300 fs depending on whether one assumes inhomogeneous or homogeneous broadening. Thus we find that the phase coherence time of a regular exciton polarization is heavily shortened by the existence of CTX states at lower energies despite the prominent regular exciton resonance feature in the linear absorption. The Coulomb attraction between electrons and holes cannot prevent the relaxation process resulting in the breakdown of the exciton correlation.

V. CONCLUSION

We study the ultrafast decay dynamics of a pure coherent CTX polarization by FWM spectroscopy. Our experiments demonstrate that internal interfaces in semiconductor heterostructures considerably affect the coherent dynamics of exciton polarizations. We find that the phase coherence time of the CTX polarization is reduced compared with the coherence time of regular excitons in a type-I reference sample due to additional scattering processes at interface imperfections. Furthermore, we show that scattering processes among CTXs are by a factor of 2 more efficient than scattering processes among regular excitons in spatially direct quantum well structures by applying a prepulse. We suggest that carrier separation in the type-II structure leads to larger spatial dipole moments and correspondingly stronger dipole-dipole interactions. Moreover, the more fermionic character of CTXs due to the spatial separation of electrons and holes may be responsible for enhanced X-X scattering in type-II quantum wells. Finally, we analyze the coherent dynamics of spatially direct exciton polarizations in the presence of a CTX state found at lower energies leading to an ultrafast loss of regular exciton polarizations.

ACKNOWLEDGMENTS

Financial support from the Deutsche Forschungsgemeinschaft through the Collaborative Research Center SFB 1083 (Project No. 223848855) as well as the European Regional Development Fund (ERDF) through the innovation laboratory high-performance materials FPG990 0005/2018 is gratefully acknowledged.

[1] K. Tomioka, M. Yoshimura, and T. Fukui, Nature (London) **488**, 189 (2012).
[2] N. G. Orji, M. Badaroglu, B. M. Barnes, C. Beitia, B. D. Bunday, U. Celano, R. J. Kline, M. Neisser, Y. Obeng, and A. Vladar, Nat. Electron. **1**, 532 (2018).
[3] H. Zhou, Q. Chen, G. Li, S. Luo, T.-B. Song, H.-S. Duan, Z. Hong, J. You, Y. Liu, and Y. Yang, Science **345**, 542 (2014).
[4] H. Chen, W. Zhang, M. Li, G. He, and X. Guo, Chem. Rev. **120**, 2879 (2020).
[5] D. Snoke, S. Denev, Y. Liu, L. Pfeiffer, and K. West, Nature (London) **418**, 754 (2002).
[6] M. Mikhailova, K. Moiseev, and Y. P. Yakovlev, Semicond. Sci. Technol. **19**, R109 (2004).
[7] H. Li, J. Tang, Y. Kang, H. Zhao, D. Fang, X. Fang, R. Chen, and Z. Wei, Appl. Phys. Lett. **113**, 233104 (2018).
[8] I. Galbraith, P. Dawson, and C. T. Foxon, Phys. Rev. B **45**, 13499 (1992).
[9] M. Koch, R. Hellmann, G. Bastian, J. Feldmann, E. O. Göbel, and P. Dawson, Phys. Rev. B **51**, 13887 (1995).
[10] T. Mishina, F. Sasaki, and Y. Masumoto, Surf. Sci. **267**, 634 (1992).
[11] K. Leo, J. Shah, E. O. Göbel, T. C. Damen, K. Köhler, and P. Ganser, Appl. Phys. Lett. **56**, 2031 (1990).
[12] N. N. Ledentsov, J. Böhrer, M. Beer, F. Heinrichsdorff, M. Grundmann, D. Bimberg, S. V. Ivanov, B. Y. Meltser, S. V. Shaposhnikov, I. N. Yassievich, N. N. Faleev, P. S. Kop'ev, and Z. I. Alferov, Phys. Rev. B **52**, 14058 (1995).
[13] M. Jo, M. Sato, S. Miyamura, H. Sasakura, H. Kumano, and I. Suemune, Nanoscale Res. Lett. **7**, 654 (2012).
[14] M. Stein, C. Lammers, P.-H. Richter, C. Fuchs, W. Stolz, M. Koch, O. Vänskä, M. J. Weseloh, M. Kira, and S. W. Koch, Phys. Rev. B **97**, 125306 (2018).
[15] M. Stein, C. Fuchs, W. Stolz, D. M. Mittleman, and M. Koch, Phys. Rev. Appl. **13**, 054073 (2020).
[16] J. Shah, *Ultrafast Spectroscopy of Semiconductors and Semiconductor Nanostructures*, Springer Series in Solid-State Sciences Vol. 115 (Springer, New York, 2013).
[17] L. Schultheis, J. Kuhl, A. Honold, and C. W. Tu, Phys. Rev. Lett. **57**, 1635 (1986).
[18] A. Honold, L. Schultheis, J. Kuhl, and C. W. Tu, Phys. Rev. B **40**, 6442 (1989).
[19] T. Yajima and Y. Taira, J. Phys. Soc. Jpn. **47**, 1620 (1979).
[20] S. T. Cundiff, Opt. Express **16**, 4639 (2008).
[21] S. W. Koch, T. Meier, F. Jahnke, and P. Thomas, Appl. Phys. A: Mater. Sci. Process. **71**, 511 (2000).
[22] C. Meineke, M. Prager, J. Hayes, Q. Wen, L. Z. Kastner, D. Schuh, K. Fritsch, O. Pronin, M. Stein, F. Schäfer, S. Chatterjee, M. Kira, R. Huber, and D. Bougeard, Light: Sci. Appl. **11**, 151 (2022).